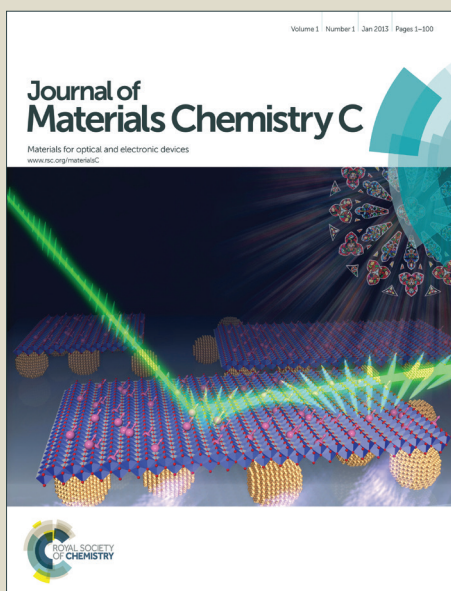


Journal of Materials Chemistry C

Accepted Manuscript



This is an *Accepted Manuscript*, which has been through the Royal Society of Chemistry peer review process and has been accepted for publication.

Accepted Manuscripts are published online shortly after acceptance, before technical editing, formatting and proof reading. Using this free service, authors can make their results available to the community, in citable form, before we publish the edited article. We will replace this *Accepted Manuscript* with the edited and formatted *Advance Article* as soon as it is available.

You can find more information about *Accepted Manuscripts* in the [Information for Authors](#).

Please note that technical editing may introduce minor changes to the text and/or graphics, which may alter content. The journal's standard [Terms & Conditions](#) and the [Ethical guidelines](#) still apply. In no event shall the Royal Society of Chemistry be held responsible for any errors or omissions in this *Accepted Manuscript* or any consequences arising from the use of any information it contains.

Chemistry of Active Oxygen in RuO_x and Its Influence on the Atomic Layer Deposition of TiO₂ Films

Cite this: DOI: 10.1039/x0xx00000x

Received 00th January 2012,
Accepted 00th January 2012

DOI: 10.1039/x0xx00000x

www.rsc.org/

Woojin Jeon,^a Woongkyu Lee,^a Yeon Woo Yoo,^a Cheol Hyun An,^a Jeong Hwan Han,^b Seong Keun Kim,^c and Cheol Seong Hwang^{a,*}

Rutile structured TiO₂ films have received great attention as a dielectric of capacitors of the next-generation dynamic random access memory (DRAM) due to its high dielectric constant (80 – 150). Ru or RuO₂, which is one of the most promising electrode materials in DRAM capacitors, is dispensable to form the rutile structure. In this work, a series of the Ru-related layers with compositions ranging from Ru to RuO₂ via RuO_x (x: ~1.12) was used as a bottom electrode for the ALD growth of TiO₂ films. It was found that the growth per cycle of TiO₂ at the initial growth stage was drastically increased on RuO_x (RuO₂/Ru mixture) compared to Ru and RuO₂. This is attributed to the drastic increase in the chemical activity of oxygen in the mixture film of RuO₂/Ru. The catalytic decomposition of RuO₂ with the help of Ru in the film played the crucial role for the increase in the active oxygen. While RuO₂ and Ru mostly retained their structures during the ALD of TiO₂ or chemical etching using O₃ gas, the RuO_x film, which was composed of 56% RuO₂ and 44% Ru, drastically changed its phase composition during the ALD of TiO₂ at 250 °C and became almost Ru. Other chemical effects depending on the chemical composition and phase structure were also examined in detail.

I. INTRODUCTION

Atomic layer deposition (ALD) is a highly intriguing thin-film growth technique with self-regulating and self-terminating properties due to the saturated chemical reactions between the adsorption sites and the chemically adsorbing precursor molecules.¹⁻⁵ Such characteristics of ALD provided the films with high uniformity over a large surface area, having an extremely topographically complicated shape and atomic-scale accuracy in thickness control. These optimal thin-film growth properties very well meet the stringent requirements of the highly scaled semiconductor fabrication processes, and as such, many of the conventional film growth processes that depend on the chemical vapour deposition (CVD) technique are now being replaced with the ALD processes,^{6, 7} although ALD was originally suggested for a thicker film growth with high thickness accuracy over a large glass surface for display application.⁸

In such ALD processes, the substrate plays a crucial role by taking part in the ALD-specific chemical reactions. The surface of the substrate must provide the chemical adsorption sites, which would anchor the incoming metal or non-metal precursors via the ligand exchange reactions. On the same line of consideration, the surface of the growing film should also provide the reaction sites for the continuous film growth while the density and chemical activity of these sites on the growing film may differ from those on the substrate. In either case, the

atoms or elements that were already incorporated into the film during the previous ALD step are generally not supposed to play an active role in the next ALD step. There are other cases, however, where the oxygen ions (or atoms) inside the film play the crucial role in the film growth. It has been reported experimentally and theoretically that many of the platinum family metals, such as Ru, Pd, Rh and Ag, come to have subsurface oxygen when the surface of these metals are saturated with adsorbed oxygen atoms by the pulse of a sufficient amount of oxygen gas.⁹ Such subsurface oxygen atoms do not form a strong chemical bond with the neighbouring metal atoms and expand the metal crystal structure, making them highly vulnerable to the chemical reaction with the ligands of the subsequently supplied MO precursors. This is the basic mechanism for the noble metal film growth even when no reducing agent was adopted; the oxygen atoms contained within the metal film surface (subsurface oxygen) strongly anchor the incoming MO precursors during the subsequent MO precursor pulse step. They eventually react with the ligands of the adsorbed MO molecules, and the reaction by-products desorb from the surface.¹⁰ Such ALD reaction route could be provided by the elegant balance between the weak chemical bonding energy of Ru-O and the stronger reactivity between the ligand and the O atoms, which were extracted from the subsurface region of the growing film.

Another example of the active role of oxygen in the substrate on the oxide film growth via ALD is the supply of oxygen atoms from the fully oxidized conducting oxides, such as RuO₂ and IrO₂, to the MO precursors adsorbing on the surface during the pulse step of the MO precursors.¹¹ This generally results in an excessively high growth rate of the oxide films at the early stage of ALD, and substantial oxide film growth even with only MO precursor pulses. This is especially serious when the metal ions in the growing oxide films have a much higher oxidation potential than Ru or Ir, and when the growth temperature is higher.¹¹⁻¹³ A typical example can be found from the SrO and TiO₂ film growth on those bottom electrode layers at a substrate temperature (T_s) of 370 °C,^{11, 12} which becomes much less severe when the T_s is decreased.¹³ Another complication regarding the substrate-oxygen-induced ALD can be found when a highly oxidizing oxygen source such as O₃ is adopted for the oxide film growth, which can induce the in-situ oxidation of the underlying Ru bottom layer.^{14, 15} For the case of the ALD of TiO₂ on the metal Ru electrode, using titaniumtetraisopropoxide (Ti(O(C₃H₇))₄, TTIP) and O₃ as the Ti precursor and oxygen source, respectively, the O₃ in situ oxidized the Ru substrate, and the resulting ~1-nm-thick RuO₂ induced the phase transition of TiO₂ from anatase to rutile through the local epitaxial relationship.¹⁴ Rutile TiO₂ thin films have a dielectric constant of ~130,¹⁶ which is the highest among the reported polycrystalline binary dielectric films with <10 nm thickness. This is an extremely promising aspect of this material for the capacitor dielectrics in the future dynamic random access memory.¹⁷ This is also the main research topic in this work, but with differently pre-processed RuO_x (0 ≤ x ≤ 2) bottom layers, which were achieved from the reduction process of the RuO₄ precursor mediated by H₂ gas.^{18, 19} Therefore, understanding the chemical environment and resulting activity of the oxygen atoms in the underlying RuO_x layer is crucially important in correctly understanding the ALD process of the TiO₂ film on top, and in improving the resulting properties.

While the most accessible method of growing Ru (or RuO_x) films must be (reactive) sputtering,²⁰ most of the highly scaled electronic devices require the conformal growth of these films, which obviously cannot be achieved through the sputtering technique. Therefore, the CVD and ALD of Ru and RuO_x films were extensively researched on in the past decades.²¹⁻²⁴ As mentioned earlier, most of these CVD and ALD processes are based on the oxidative decomposition of the Ru MO precursors for CVD or on the repeated oxidation-reduction of the growing layers for ALD.

Recently, an alternative chemical route for the synthesis of the thin films of Ru and RuO₂ was demonstrated based on the thermal decomposition of RuO₄, which is an inorganic Ru precursor whose various physical parameters are quite similar to those of Al(CH₃)₃, except for the low thermal decomposition temperature (~150 °C).^{18, 19} Such a low thermal decomposition temperature prohibited the ALD-type growth behaviour at T_s > ~150 °C. The deposition of Ru or RuO₂ films, however, can be well controlled in a self-saturating manner by the enhancement of the chemical adsorption of RuO₄ on the H₂-pulsed surface in the pulsed CVD (p-CVD) process.¹⁸ The primary by-product of the thermal decomposition of RuO₄ is RuO₂, which can be further reduced to metallic Ru with the help of H₂ gas. When a Ru seed is formed in the RuO₂ layer, it catalyses the further reduction of RuO₂ to Ru, in addition to the enhancement of RuO₂ deposition by the Ru nuclei (or seed) via the RuO₄ + Ru → 2RuO₂ reaction route. There can be an intermediate phase,

however, RuO_x (0 < x < 2), when the H₂ reduction process is appropriately controlled, but its thermal stability must be quite limited. It must be an interesting task, therefore, to examine the influence of this intermediate phase on the ALD of the TiO₂ film as well as its own variation. It can also be anticipated that this intermediate phase may show rather complicated in-situ reactions with the oxygen source in TiO₂ ALD, which was O₃ in this work, making the accurate understanding of the reaction kinetics even more challenging.

In this work, therefore, the three different phases of Ru, RuO_x (x: ~1.12), and RuO₂ were grown by carefully controlling the H₂(5%)/N₂(95%) reduction gas pulse time during the p-CVD using RuO₄ as the Ru precursor at a 230 °C T_s. The influence of these phases on the sub-sequent ALD process of TiO₂ was carefully studied to reveal the role of the active “solid” oxygen contained by the underlying RuO_x layer.

II. EXPERIMENTAL PROCEDURE

RuO₂ films were deposited via p-CVD using a RuO₄ precursor dissolved in a blend of organic solvents containing fluorinated solvents (ToRuS, total ruthenium solution, produced by Air Liquide Co., with a 0.8 M concentration) and 95% N₂/5% H₂ mixed gas (N₂/H₂) as the Ru precursor and reactant gas, respectively. The deposition temperature was 230 °C, and the p-CVD sequence consisted of four steps: Ru precursor injection (0.5 s) – Ar purge (7 s) – N₂/H₂ gas injection (1-10 s) – Ar purge (5 s). The N₂/H₂ reactant exposure time was controlled to produce the desirable oxygen composition of Ru films. The Ru solution was cooled down to 3 °C to achieve an appropriate vapour pressure, and no carrier gas was used to introduce the precursor molecules into the p-CVD chamber. A more detailed description of the deposition procedure of Ru and RuO₂ films using RuO₄ was reported elsewhere.^{18, 19} The flow rate of the N₂/H₂ gas was fixed to 100 sccm. 5 nm Ta₂O₅ deposited on Si wafer via CVD was used as the substrate for Ru, RuO_x, and RuO₂ film growth. The ALD TiO₂ films were deposited using TTIP and O₃ (250 g/m³) as the Ti precursor and oxygen source, respectively, and the sequence consisted of the TTIP feeding (3 s) – Ar purge (5 s) – O₃ feeding (3 s) – Ar purge (5 s) steps at the growth temperature of 250 °C. Ru, RuO_x and RuO₂ films were deposited immediately prior to the TiO₂ ALD. There must be some additional oxygen adsorbed on the film surface, but this must be much less significant compared with the inherently included oxygen concentration in the film. Therefore, it must be safe to ignore the surface contamination effect. The modified TiO₂ ALD sequences were also conducted, such as the TTIP-only sequence, which consisted of TTIP feeding (3 s) – Ar purge (5 s) – Ar purge (3 s, instead of O₃) – Ar purge (5 s), or the O₃ pretreatment sequence, which consisted of several cycles of O₃ feeding (3 s) – Ar purge (13 s) before normal TiO₂ ALD. The modified sequences were designed to ensure the same process conditions, such as the process time, thermal budget, and chamber pressure, as that of the normal TiO₂ ALD.

The film thickness of both the Ru and TiO₂ films were determined through calculation from the layer density, which was measured via X-ray fluorescence spectroscopy (XRF, Thermoscientific, ARL Quant’X), and the film density via X-ray reflectivity (XRR, PANalytical, X’pert Pro.). XRR was used to estimate the film thickness too for several cases. XRF cannot detect oxygen so that the estimated layer density of Ru or Ti was used to check the amount of the deposited RuO₂ or TiO₂ film, respectively. The chemical properties of the RuO_x films were checked via X-ray photoelectron spectroscopy

(XPS, VG, Sigma Probe). The depth profiles of the films were analysed via time-of-flight medium energy ion scattering spectroscopy (ToF-MEIS, K-MAC, MEIS-K120) using a He-ion beam with an acceleration energy of 100 keV. Glancing angle incident X-ray diffraction (GAXRD, PANalytical, X'pert Pro., incidence angle of 0.5°) was used to examine the crystallographic structure of the deposited films. The surface morphology and roughness were observed via atomic force microscopy (AFM, JEOL, JSPM 5300).

III. RESULTS AND DISCUSSION

Figure 1 shows the variations in the (a) film thickness and bulk density (both evaluated from XRR) and (b) resistivity (sheet resistance measured via four-point probe and film thickness) and surface roughness (via XRR) of the deposited RuO_x ($0 \leq x \leq 2$) film properties as a function of the N_2/H_2 reactant feeding time ($t_{\text{N/H}}$), which was varied from 1 to 10 sec. Here, the p-CVD cycle was repeated 90 times for all the cases. When the $t_{\text{N/H}}$ was as short as 1 sec, the film thickness was very low, suggesting that the film deposition was inefficient under this condition. When the $t_{\text{N/H}}$ increased to 5 sec, the film thickness largely increased, which can be understood from the enhanced efficiency for decomposing RuO_4 to RuO_2 with the help of the H_2 gas adsorbed on the growing film surface.²⁵ When the $t_{\text{N/H}}$ increased to over 7 sec, the film thickness decreased drastically. This does not mean, however, that the p-CVD reaction is retarded under this condition; this is due to the largely increased film density, as can be understood from the red-coloured data points in the same figure. Such a variation in the film density and thickness can be well correlated with the variations in the film resistivity shown in Fig. 1(b), where the resistivity was quite high and low when the density was low (the thickness was high) and high (the thickness was low), respectively. These variations are consistent with those in the previous report,¹⁸ which indicates that the films with a low $t_{\text{N/H}}$ (<5 sec) were RuO_2 whereas the films with a high $t_{\text{N/H}}$ (>5 sec) were Ru, although the transition $t_{\text{N/H}}$ value (~ 6 sec) was slightly different from that in the previous report (~ 11 sec). Such difference can be ascribed to the different RuO_4 concentration in the ToRuS solution (0.8 M in the present work vs. 1.6 M in the previous work). The different phases of the grown films for the two distinctive $t_{\text{N/H}}$ regions (RuO_2 vs. Ru) can also be confirmed in this work (the data in Fig. 2 and the related discussions). The largely increased roughness of the Ru films for $t_{\text{N/H}} > 5$ sec can be ascribed to the highly enhanced incorporation speed of the Ru metal atoms from the autocatalytic effect of the Ru clusters for the reduction reaction of RuO_2 to Ru. These observations are quite similar to those in the previous report.¹⁸ In order to check the phases of TiO_2 film on the three types of substrate, the dielectric constants of the dielectric films, which were grown by a common cycle number of 200, were estimated. They were 104.1, 103.4, and 102.2 for the t4, t5, and t10 samples respectively. For this electrical test, the Pt top electrode (~ 0.3 mm in diameter) was deposited by a DC sputtering method through metal shadow mask. XRD was not successful to distinguish the phases because the TiO_2 film thicknesses were too thin ($< 8 - 9$ nm) to show evident diffraction peaks.

A peculiar finding could be made, however, from the high resistivity of the film at $t_{\text{N/H}} = 5$ sec, whose resistivity was as high as $334 \Omega \cdot \text{cm}$ whereas those of the films with the RuO_2 and Ru phases were 230-280 and 25-30 $\Omega \cdot \text{cm}$, respectively. This

strongly suggests that something uncommon occurred at the condition of $t_{\text{N/H}} = 5$ sec. Moreover, the ALD TiO_2 film on these films were also exhibited extraordinary growth behaviour. Figure 1(c) shows the variations in the Ti layer density as a function of the number of TiO_2 ALD cycles (n_{cy}) for the three different substrates with $t_{\text{N/H}} = 4, 5,$ and 10 sec (the samples named "t4," "t5," and "t10"), respectively, and Fig. 1(d) shows the growth rate of the Ti layer density as a function of n_{cy} , which could be acquired by differentiating the data in Fig. 1(c). There was hardly any incubation cycle (n_{cy} , where TiO_2 did not grow during the initial ALD stage), suggesting the good nucleation property of TiO_2 films on these substrates. Figure 1(d) clearly revealed that the substrates generally enhanced the TiO_2 film deposition, where the enhancement was retained up to 40-50 cycles for samples t4 and t10, whereas the effect was retained up to 100 cycles for the case of sample t5. The

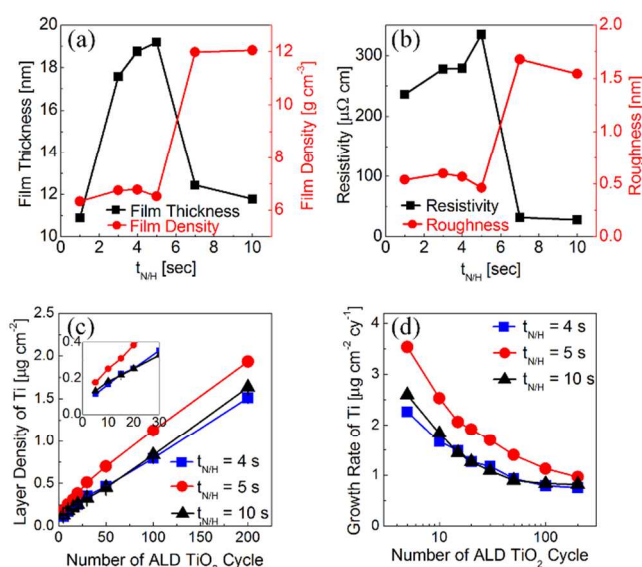


Figure 1. (a) Variations of film thickness and its density, and (b) resistivity and roughness values of deposited RuO_x ($0 \leq x \leq 2$) as a function of N_2/H_2 reactant feeding time. The comparison of (c) layer density and (d) differentiating growth rate of TiO_2 films as a function of deposition cycles deposited on samples of t4, t5, and t10.

enhancement of TiO_2 growth in the low- n_{cy} region on the RuO_2 and Ru electrodes has been reported elsewhere, which has been understood from the CVD-like reaction of $\text{Ti}(\text{O-iPr})_2(\text{tmhd})_2$ ¹¹ or TTIP²⁶ molecules on the RuO_2 surface when the precursor molecules were pulsed. In the genuine ALD reaction route, there should be no oxide formation at this step; only the chemical adsorption of the precursor molecules, whose degree is largely determined by the steric hindrance effect and surface density of the chemisorption sites. When the substrate provided the adsorbing molecules with active oxygen atoms, however, the oxide layer was formed even at the precursor pulse step, which resulted in an enhanced growth rate. This type of CVD-like reaction must be retarded as the substrate surface came to be covered with the growing film because the chemical interaction between the RuO_2 substrate and the TTIP molecules was interfered with by the growing film.

Nevertheless, the interaction could be maintained up to a certain TiO_2 film thickness because the oxygen dissociated from O_3 during the O_3 pulse step could be diffused into the underlying RuO_2 layer through the grown TiO_2 layer, which

could be diffused back to the film surface and could react with the TTIP molecules during the subsequent TTIP pulse step.¹³ An identical mechanism could be used to explain the growth enhancement on Ru given the fact that Ru can be oxidized to RuO_x (or even RuO_2) during the O_3 pulse step.

The much higher enhancement of TiO_2 film growth on sample t5, which was preserved up to the n_{cy} of 100, manifested that there is another factor that further enhances the TiO_2 growth rate. To confirm such peculiarity, the physical and chemical properties of t4, t5, and t10 were examined in detail. The chemical structures of the films were evaluated using XPS analysis. Figures 2(a)–(c) show the Ru 3d XPS spectra (data points) of t4, t5, and t10, respectively. Also shown in the same figures are the deconvoluted spectra (lines) assuming the Ru 3d peaks were composed of Ru $3d_{5/2}$ peaks centred at the 280.0, 280.8, and 281.8 eV binding energies (BE), which correspond to metallic Ru, RuO_2 , and RuO_3 , respectively. For the t4 sample,

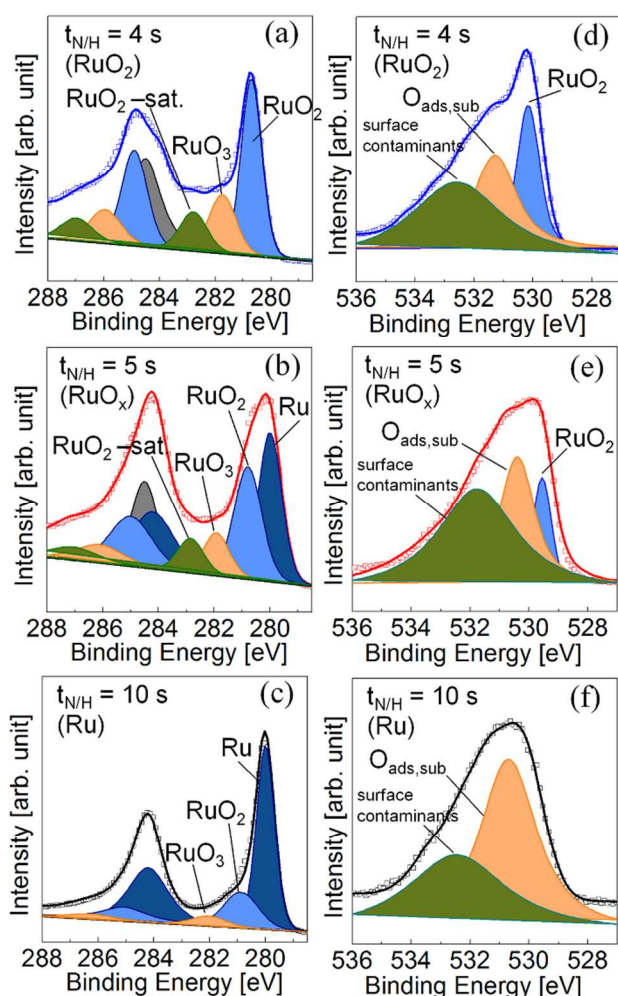


Figure 2. Peak fits of (a)–(c) Ru3d spectra and (d)–(f) O1s spectra of t4, t5, and t10 on as-deposited films. In Ru3d spectra, deconvoluted carbon peak is indicated as black colour, and left-side peaks are originated from $3d_{3/2}$. Peak deconvolution was conducted with $3d_{5/2}$ spectra (right-side peaks).

the Ru 3d peak was mainly composed of the peak with a 280.8 eV BE and a minor contribution from the peak with a 281.8 eV BE, suggesting that the film was mainly RuO_2 . RuO_3 might

have been present on the film surface due to the dissociative adsorption of O_2 or H_2O .²⁷ The peak located about 282.5 eV denoted the extended RuO_2 composition, which was called as RuO_2 satellite.¹⁰ In contrast, the main contribution to the Ru 3d XPS peak was made from the peak with a 280.0 eV BE for the t10 case, suggesting that the film was mainly Ru. The minor peaks located at 280.8 and 281.8 eV could also have been from the surface-oxidized layer. Sample t5 shows the intermediate composition of the Ru 3d peak, as expected, where the peaks with 280.0 and 280.8 eV BEs had relatively similar contributions to the total intensity. This reveals that the t5 sample was composed of a mixture of RuO_2 and Ru. Such identification of the films was further confirmed by the O 1s XPS spectra shown in Figures 2(d)–(f) for the same samples. The O 1s spectra were also deconvoluted assuming the presence of peaks located at the 529.5, 530.7, and ~ 532 eV BEs, which correspond to the oxygen in the bulk RuO_2 , the surface adsorbed or subsurface oxygen ($\text{O}_{\text{ads,sub}}$), and surface contamination, such as water or hydrocarbons, respectively. The presence of $\text{O}_{\text{ads,sub}}$ has been reported experimentally^{10, 28–30} and theoretically^{9, 31} which coincide with the oxygen atoms without forming strong chemical bonds with Ru, as in RuO_2 . Considering the reaction kinetics of RuO_2 and Ru film formation through the reductive routes in this work ($\text{RuO}_4 \rightarrow$

$\text{RuO}_2 + \text{O}_2$, $\text{RuO}_2 \rightarrow \text{Ru} + \text{O}_2$, and $\text{RuO}_4 + \text{Ru} \rightarrow 2\text{RuO}_2$), it is not extraordinary to consider the involvement of the RuO_x phase, where x is < 2 , in the middle of the CVD reaction. The O 1s spectrum of sample t4 showed a strong and sharp peak at 529.5 eV BE, suggesting that the film is mainly well-crystallized RuO_2 . The t10 sample showed a much weaker O 1s peak intensity, which coincides with the fact that t10 was mainly of the Ru phase. The deconvoluted O 1s spectrum clearly revealed that there was an evident peak at 530.7 eV BE with strong intensity, suggesting that the sufficient amount of $\text{O}_{\text{ads,sub}}$ was clearly present in this sample. The deconvoluted peaks of O 1s spectrum of sample t5 (Fig. 2(e)) evidently showed simultaneous involvements of the Ru and RuO_2 phases. The coexistence of RuO_2 and Ru with $\text{O}_{\text{ads,sub}}$ atoms has an important implication on the ALD of the TiO_2 film on top, as will be shown later; the RuO_2 phase decomposed to Ru and oxygen, which provided the incoming TTIP molecules with active oxygen atoms even before the O_3 pulse was made.

Figure 3(a) shows the ToF-MEIS depth profiles for oxygen of the three films at the as-deposited states. The high oxygen concentration at depth 10 – 15 nm of sample t10 corresponds to the Ta_2O_5 substrate layer, which was observed at depth 20 – 25 nm for the other two cases. These results corroborate the fact that the thickness of the Ru film in sample t10 is much lower than those of the other two (Fig. 1(a)). As expected, sample t4 had the highest oxygen concentration, and sample t10 almost negligible oxygen concentration, except for its surface, due to the contamination and surface adsorbed oxygen. Sample t5 had an intermediate oxygen concentration, which was closer to that of t4 than t10. The O/Ru ratio of sample t5, estimated from the oxygen concentration in the middle of the layer, was ~ 1.12 which suggests that the RuO_2 : Ru phase ratio was obtained as 0.56 : 0.44, assuming the stoichiometric RuO_2 and negligible oxygen concentration in the Ru phase. To understand what occurred in the chemical states of these films during the ALD steps, the following experiments were performed on these three samples, and the oxygen depth profiles were again examined. First, the five cycles of TiO_2 ALD (the TTIP and O_3 pulses) were performed, and the oxygen profiles are shown in figure

3(b). The high oxygen concentration of the film surface can be ascribed to the presence of a very thin TiO_2 layer (with a 0.15 nm nominal thickness, estimated from the saturated ALD rate of $\text{TiO}_2 \sim 0.03$ nm/cycle). While the bulk of the Ru layer in t10 remained almost oxygen-free (black line), the oxygen concentration of both samples t4 and t5 decreased significantly after only five cycles of TiO_2 ALD. The decrease was the most significant for the case of t5 (Fig. 3(e)), suggesting that the oxygen in sample t5 was the most vulnerable to the removal probably by the reaction with TTIP. Figure 3(c) shows the oxygen signal depth profiles of the three samples after the O_3 pretreatments (no TTIP pulse). Sample t10 showed a high oxygen signal on the surface, and the bulk region showed only a marginally increased concentration. This suggests that sample t10 had a relatively high resistance to infiltration of oxygen, which can be ascribed to the high crystalline quality of the Ru film in this sample. Samples t4 and t5 showed quite notable changes after the O_3 pretreatments; the oxygen concentration of sample t5 (Fig. 3(e)) was increased both bulk region and

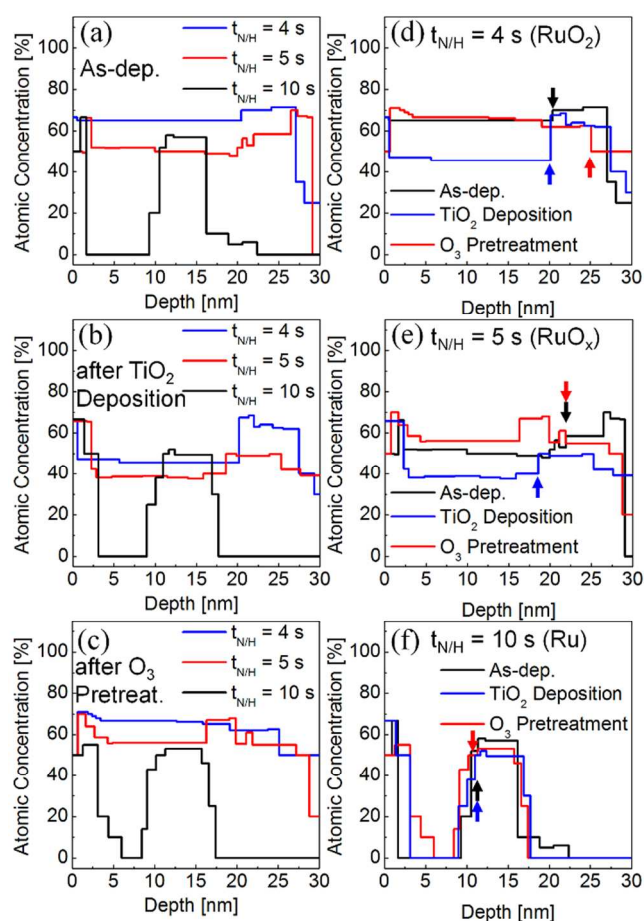


Figure 3. Depth profile of oxygen atom, where (a) as-deposited, (b) after five cycles of TiO_2 ALD and (c) after the O_3 pretreatment, and oxygen profile change in (d) t4, (e) t5 and (f) t10 by subsequent process, analysed by time-of-flight medium energy ion scattering spectroscopy. Coloured arrows in (d)-(f) indicate the interface between RuO_2 (or Ru) on left-side and Ta_2O_5 layer on right-side.

interface, while the sample t4 (Fig. 3(d)) exhibited no significant change. The slight increase in oxygen signal of t5 can be ascribed to the further oxidation of the Ru phase to RuO_2 . The large variation in the oxygen concentration after the

ALD of TiO_2 (shown in Fig. 3(b)) appeared to have a close relationship with the phase evolution of t4, t5, and t10 during the ALD, and the variations in the initial ALD speed. Figure 3(f) showed that the oxygen behaviour in sample t10 was not deviated from the usual expectation; bulk of Ru layer remained almost oxygen-free and only surface contained oxygen atoms. The chemical composition of Ru, RuO_x and RuO_2 layer after the deposition of TiO_2 films by 10 cycles was also checked by XPS. The results were identical to the MEIS results of Fig. 3 (data not shown).

Figure 4 shows the GAXRD spectra of samples t4, t5, and t10 before and after the 10 cycles of TiO_2 ALD. All the as-deposited films were crystallized without any post-deposition annealing. The diffraction peaks from the as-deposited sample t4 indicated that the thin film had crystalline RuO_2 with a rutile structure [(110) at $2\theta \sim 27.9^\circ$ and (111) at 40.6°]. Metallic Ru peaks were detected at $2\theta \sim 38.8^\circ$ for (100), 42.5° for (002), and 44.4° for (101) from sample t10. No significant change in the diffraction pattern was observed even after the deposition of 10 ALD cycles of TiO_2 in both samples t4 and t10. The nominal thickness of the TiO_2 layer was only 0.3 nm, and as such, the TiO_2 layer could not show any diffraction peak from this GAXRD setup but can just slightly mask the underlying layers from the incident X-ray. In contrast to samples t4 and t10,

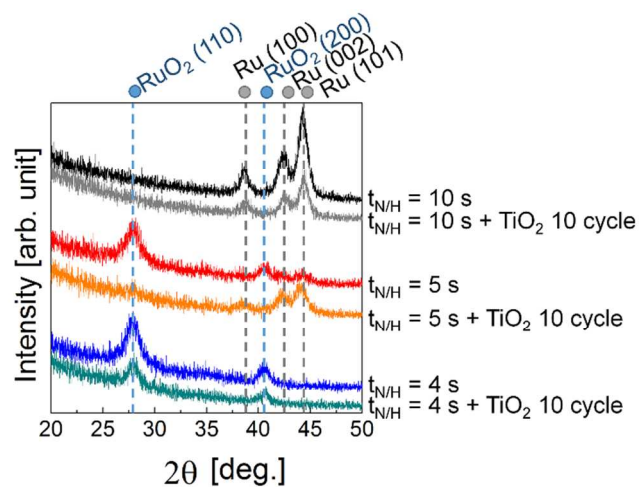


Figure 4. Glancing angle incident X-ray diffraction spectra of t4, t5, and t10 substrates, and after 10 cycles of TiO_2 deposition on each substrates.

Table I. GAXRD peak positions (2θ) of the three samples at the as-deposited state and after the 10 cycles of TiO_2 ALD.

Samples	RuO_2 (110)	Ru (100)	RuO_2 (111)	Ru (002)	Ru (101)
10 s		38.75		42.48	44.32
10 s + TiO_2 10cy		38.71		42.48	44.40
5 s	27.94		40.56	42.16	44.13
5 s + TiO_2 10cy	27.94	38.35		42.29	44.09
4 s	27.85		40.59		
4 s + TiO_2 10cy	27.83		40.57		

sample t5 showed diffraction peaks at $2\theta \sim 27.9$ and 40.6° , which corresponded to RuO_2 , as well as peaks at $2\theta \sim 42.2$ and 44.1° , which corresponded to Ru, at the as-deposited state, although the Ru peaks were much weaker than that of sample t10. This phase composition corroborates the above XPS results. Despite the low peak intensities, the positions of each peak can be determined by fitting the spectra with the Gaussian function. The estimated peak positions are summarized in Table I. It can be understood that in addition to the coexistence of RuO_2 and Ru in sample t5, the peak positions of the Ru phase are certainly shifted into the lower 2θ direction by $0.2\text{--}0.3^\circ$ compared with t10, whereas that of the RuO_2 peak showed a smaller shift into the higher 2θ direction by $\sim 0.1^\circ$ compared with sample t4. This suggests that the Ru phase in sample t5 had an increased lattice parameter, probably due to the remaining oxygen in the metallic Ru lattice, while the RuO_2 in sample t5 had a slightly decreased lattice parameter, but it was less obvious compared with that of Ru. In this regard, it is supposed to be that the Ru phase in sample t5 had the high concentration of $\text{O}_{\text{ads,sub}}$. Another notable finding could be obtained from the GAXRD spectrum of sample t5 after the 10 ALD cycles of TiO_2 ; the RuO_2 peak disappeared almost completely while the Ru peaks quite notably increased in intensity, with their shifted peak positions maintained. This suggests that the catalytic decomposition of RuO_2 to Ru with the help of the presence of Ru occurred during the ALD of TiO_2 on top in this case, as discussed in ToF-MEIS analysis.

The results shown in figures 2-4 well corroborate the previously reported mechanisms for the RuO_2 and Ru film deposition using the RuO_4 and N_2/H_2 gas as the Ru precursor and reduction agent.¹⁸ RuO_4 could be thermally decomposed at this temperature (230°C) to form RuO_2 , but the addition of H_2 gas enhances the chemical adsorption of RuO_4 on the H_2 -adsorbed RuO_2 film surface, increasing the RuO_2 growth rate. During the long $t_{\text{N/H}}$, the deposited RuO_2 decomposed to Ru while the oxygen atoms were removed by the reaction with H_2 . There was a catalytic activity of Ru that further enhanced the RuO_2 reduction when the Ru nuclei were formed. This resulted in the abrupt phase transition of the depositing film from RuO_2 to Ru at a certain critical $t_{\text{N/H}}$ (~ 6 sec in this case, and ~ 11 sec in Ref. 18) When the deposited film became Ru (due to the sufficiently long $t_{\text{N/H}}$), the deposition of the film during the subsequent RuO_4 pulse step was further enhanced by the reaction $\text{RuO}_4 + \text{Ru} \rightarrow 2\text{RuO}_2$, and the resulting RuO_2 was reduced to Ru during the subsequent N_2/H_2 pulse step. The added knowledge in this work was the revelation of the intermediate step of the transition from RuO_2 to Ru (sample t5). The 5 sec $t_{\text{N/H}}$ appeared to be just enough time to induce the reduction of RuO_2 to Ru but not long enough to induce the full transformation to Ru. Therefore, the microstructure must be a physical mixture of RuO_2 and Ru (with non-negligible amount of $\text{O}_{\text{ads,sub}}$), which induced the abnormally high resistivity in this case (Fig. 1 (b)) due to the boundary scattering of electrons between the two phases. The drastic decrease in the RuO_2 phase XRD peak and the increase in the Ru phase XRD peak shown in figure 4 after the 10 ALD cycles of TiO_2 for the case of sample t5 manifested what could be the more detailed mechanism for the reduction of RuO_2 with the help of Ru. When pure RuO_2 was thermally treated under the N_2/H_2 atmosphere for a short time ($t_{\text{N/H}} < 4$ sec), which was not sufficiently long to induce Ru nuclei formation, N_2/H_2 did not seem to play any crucial role in the reduction. It just increased the RuO_4 chemisorption perhaps through the reaction 4H

(surface) + $\text{RuO}_4 \rightarrow \text{RuO}_2 + 2\text{H}_2\text{O}$ (desorption). Once the Ru nuclei started to form with the increase in $t_{\text{N/H}}$ (> 5 sec), however, they could take the oxygen from the nearby RuO_2 grains, and the acquired oxygen atoms in the Ru grains ($\text{O}_{\text{ads,sub}}$) could leave the film rapidly because $\text{O}_{\text{ads,sub}}$ was unstable. The direct extraction of oxygen atoms from RuO_2 by thermal energy (or even with the help of H_2 gas) at $200\text{--}250^\circ\text{C}$ appears quite unlikely due to the phase stability of RuO_2 . The GAXRD data shown in figure 4 for sample t4 reveal this point. When TTIP was pulsed on the film surface, it could take oxygen from the underlying layer if the binding energy between the oxygen and Ru was weaker than the Ti-O bond or even C-O (and other possible reactions between the ligands and oxygen). The Ti-O bond is much stronger than the Ru-O bond at the ALD temperature, and as such, in principle, RuO_2 reduction could occur during the TiO_2 ALD, which was indeed observed when the ALD temperature was 370°C .¹¹ The temperature of TiO_2 ALD is the critical factor that influences the growth behaviors on the different types of substrate layer. At 370°C , the catalytic decomposition of RuO_2 during the TiO_2 ALD was highly activated by the thermal energy,¹¹ so that the TiO_2 film growth rate on RuO_2 , which is the substrate layer with the highest oxygen content among the three types of Ru-O films, showed the highest growth rate. However, at a much lower ALD TiO_2 temperature of 250°C , the thermal decomposition effect of the stable RuO_2 was much less severe, so that the inherently chemical activity of subsurface oxygen atoms in the RuO_x showed the highest chemical activity. At such a relatively low ALD temperature of 250°C in this work, however, this reaction seemed to be kinetically limited, and as such, a substantial fraction of RuO_2 remained after the TiO_2 ALD for the case of sample t4. The identical growth behaviour on sample t4 and t10 can be explained as follows. Sample t10 had a negligible amount of oxygen in the bulk of the film, so it had no reason to show such an effect during the ALD of TiO_2 on top of it. However, thin RuO_2 could be grown on the Ru surface by its exposure to O_3 -containing environment.¹⁴ Only a few layers of RuO_2 , which derived the formation of rutile-structure TiO_2 on the Ru electrode when O_3 was adopted as the oxygen source, can contribute the over-growth of TiO_2 . Therefore, the t10 exhibited almost identical growth behaviour to sample t4. The availability of a catalytic reduction route for the case of sample t5 via the transfer of oxygen from RuO_2 to Ru, however, greatly facilitated the reduction of RuO_2 . When the TTIP was pulsed, the reaction by-product of the reduction reaction ($\text{RuO}_2 \rightarrow \text{Ru} + \text{O}_2$), O atoms or O_2 molecules, could be easily taken up by the TTIP, which would further enhance the reduction reaction. As a result, the RuO_2 phase seemed to be completely disintegrated even after only 10 ALD cycles on top (Fig. 4). However, the enhanced growth rate was maintained almost 100 cycles of TiO_2 deposition. As aforementioned, the adsorbed TTIP molecules were oxidized by the oxygen atoms provided by the catalytic decomposition of RuO_2 due to the coexistence of Ru in the substrate layer in case of sample t5, which is suggested by the data shown in figures 3 and 4. It is also possible that the reduced Ru could be oxidized back to RuO_2 during the O_3 pulse time, but the incorporated oxygen atoms would be diffused outward again to the film surface during the subsequent step. Actually, even after conducting 100 cycles of TiO_2 ALD, oxygen concentration of RuO_x was ~ 33 at.% (Fig. 5), which was comparable to that after five cycles of TiO_2 ALD (Fig. 3(e)).

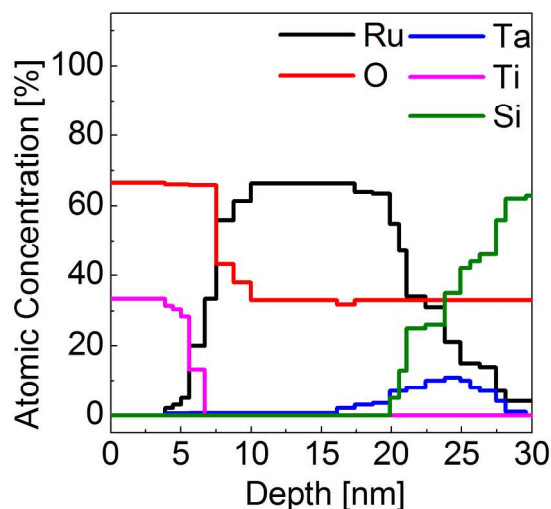


Figure 5. Depth profile of RuO_x ($t_{\text{N/H}} = 5$ sec) film after conducting 100 cycles of TiO_2 ALD.

In contrast, sample t4 showed only a marginal increase in growth rate, which was almost comparable to that of sample t10, and the Ru and RuO_2 phase remained intact after the TiO_2 ALD. These factors revealed that RuO_2 was not decomposed to Ru under these ALD conditions, which can be ascribed to the structural stability of RuO_2 . It could be easily anticipated that such a drastically different evolution of oxygen from the substrate layer during the ALD of TiO_2 would result in different ALD behaviours for the given TiO_2 ALD conditions, which was indeed the case, as shown in figures 1(c)-(d).

The interaction between O_3 and the three samples was further examined in the following manner: the three samples were treated under the O_3 pulse sequence, which was identical to the TiO_2 ALD process (without the TTIP pulse steps). Figure 6(a) shows the variation in the Ru layer density as a function of the O_3 pulse number for the three samples. While the Ru layer density decreased only marginally (<11%) for the case of sample t4, even after 7 cycles of O_3 treatment, the Ru layer density of sample t10 decreased by almost 97%. It has been reported that the Ru etching by O_3 proceeded via the reaction $\text{RuO}^* + \text{O}_3 \rightarrow \text{RuO}_4$,³² where RuO^* coincided with the Ru atoms with the nearby O atoms existing as the forms adsorbed on the surface or subsurface region, which has been represented by $\text{O}_{\text{ads,sub}}$ in this work. When the film had a stable form of RuO_2 , the reactivity of this layer towards the reaction with O_3 must have been quite limited, and no significant etching was observed.^{32, 33} The GAXRD data shown in figure 6(b) before and after the five O_3 pulse cycles revealed that there was also no major change in the phase composition. In contrast, as confirmed by the XPS spectra in figure 2, the Ru film surface (sample t10) had $\text{O}_{\text{ads,sub}}$, which could be preserved even after the O_3 pulse step, so that the etching must be quite active. The GAXRD data shown in figure 6(d) also revealed that there was no major change in the phase composition in this case. It is interesting to note that these etching and GAXRD data indicate that the RuO_2 layer was not majorly formed during the O_3 pulse step. It can be imagined that the formation of RuO_2 , which can be induced by the reaction between the Ru and O radicals

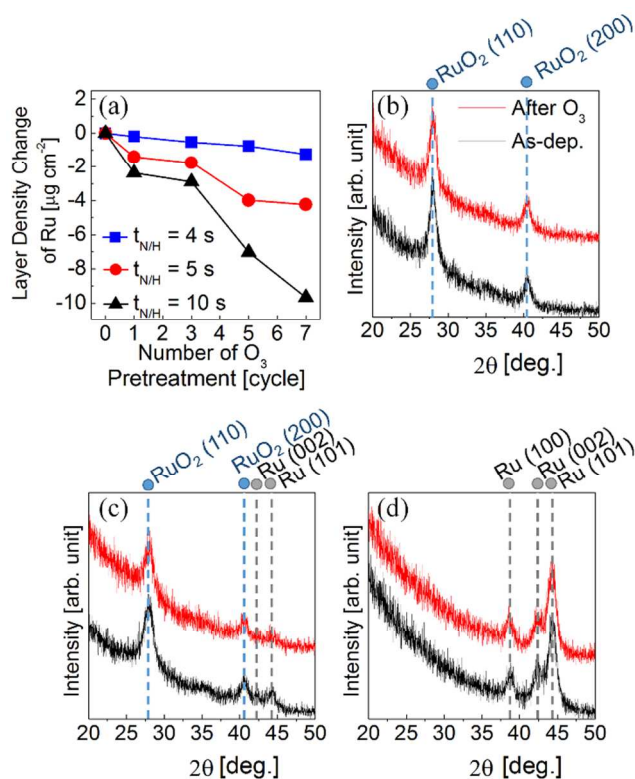


Figure 6. (a) Comparison of variations of Ru layer density of sample t4, t5, and t10 as a function of conducted cycle number of O_3 pretreatment. Glancing angle incident X-ray diffraction patterns of (b) t4, (c) t5, and (d) t10 before and after five cycles of O_3 pretreatment.

dissociated from O_3 , is in competition with the formation of RuO_4 by the aforementioned reaction. In addition, the formation of a RuO_2 layer requires the substantial rearrangement of the Ru atoms from the metal Ru structure (hexagonal close packing) to the rutile RuO_2 structure (tetragonal), which must be kinetically limited by the relatively low temperature (250 °C). When the Ru film surface was directly exposed to O_3 gas, the volatilization reaction by RuO_4 formation must have been dominant.³⁰ When the TTIP precursors were also pulsed, however, to grow ALD TiO_2 films on the Ru electrode, the desorption of RuO_4 must have been suppressed by the presence of a thin TiO_2 layer on top of the Ru surface, whereas the dissociation of O_3 to O_2 and O radical on the TiO_2 surface could be enhanced.¹⁴ The produced O radicals could be readily diffused to the underlying Ru layer and could have formed an interfacial RuO_2 layer, which is the driving force for transforming the structure of the TiO_2 clusters from either amorphous or anatase (which must be the first formed phase considering the low ALD temperature and thermodynamic condition) to a rutile structure. The formation of rutile-structure TiO_2 on the Ru electrode when O_3 was adopted as the oxygen source has been repeatedly reported.^{12, 14, 15, 26, 34, 35}

The etching behaviour of sample t5 was in between those of samples t4 and t10. The general trend, however, follows that of sample t10, suggesting that the Ru phase in sample t5 was mainly etched. Figure 6(c) shows the GAXRD pattern of sample t5 before and after O_3 etching. It will be noted that the peaks related with the Ru phase almost disappeared while the peaks related with the RuO_2 phase remained invariant after O_3

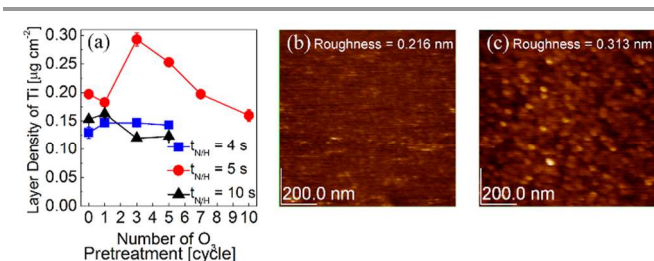


Figure 7. Comparison of deposited TiO₂ layer density on t₄, t₅, and t₁₀ substrates as a function of cycle number of O₃ pretreatment. Atomic force microscopy images of (b) before and (c) after three cycles of O₃ pretreatment on the sample of t₅.

etching. This clearly indicates that the main etching part in sample t₅ was Ru while the RuO₂ phase remained unetched.

The effects of O₃ pretreatment on the subsequent TiO₂ ALD were examined by depositing five ALD TiO₂ cycles on the O₃-pretreated samples with different treatment cycles. Figure 7(a) shows the variations in the Ti layer density as a function of the O₃ pretreatment number for the three samples. Sample t₄ did not show any notable variation in the Ti layer density up to the pretreatment cycle number of 5, except for a small increase after the first cycle, which can be attributed to the slightly increased oxygen concentration on the film surface. Sample t₁₀ first showed an increase and then a decrease after three cycles. The first increase can be understood in the same manner as for sample t₄, and the obvious decrease in Ti layer density after three cycles may be understood from the large removal of the Ru material itself after these treatments. The less the Ru that is left with the increasing O₃ pretreatment cycle number, the less oxygen could be stuffed in the remaining Ru layer, and thus, the less enhancement in TiO₂ ALD. Sample t₅ showed a rather complicated behaviour; up to three O₃ pretreatment cycles, the Ti layer density largely increased, but it finally decreased to the value of sample t₄ after 10 O₃ pre-treatment cycles. The first large increase may be understood from the increased surface area as the Ru phase was etched away by the O₃ pretreatment cycles. Figures 7(b) and (c) show the AFM topographic images of the as-deposited sample t₅ and after three O₃ pretreatment cycles, respectively. It can be understood that the structural change on the RuO_x film surface was made by the O₃ pretreatment cycles. On this surface, there was a remaining Ru phase, which was a very active source of oxygen to the incoming TTIP molecules. The fact that the Ru phase has elongated lattice and the O_{ads,sub} in its lattice may also enhance transformation of Ru to RuO₂,^{29, 30} and this RuO₂ could be contributed to oxidation of TTIP molecules by reduction reaction (RuO₂ → Ru + O₂). This is because the TiO₂ overgrowth was retained up to 100 cycles for the case of sample t₅. As the Ru phases etched away, the surface became more like RuO₂, and the TiO₂ growth rate converged to that on RuO₂ (sample t₄).

IV. CONCLUSIONS

The chemical states of RuO₂ and Ru films as the bottom electrode for the high-dielectric-rutile TiO₂ thin film, which were deposited via pulsed chemical vapour deposition (p-CVD) based on the reduction reaction of RuO₄ induced by the N₂/H₂ gas mixture, were examined in detail. When the t_{NH} was shorter than 4 sec and longer than 6 sec, the deposited films were almost single-phase RuO₂ and Ru, respectively. The film grown

at 5 sec t_{NH}, however, was identified to have had a mixture of the RuO₂ and Ru phases, where this Ru was the metallic Ru phase with an elongated lattice parameter due to the incorporation of subsurface oxygen atoms. The coexistence of the two phases in a single film drastically increased the chemical activity of oxygen in the film, largely increasing the ALD speed of TiO₂ on top up to 100 ALD cycles. This was understood as the catalytic decomposition of RuO₂ into Ru and oxygen atoms with the help of the Ru phase. The RuO₂ film had a high immunity to the chemical etching activity of O₃ due to its structural stability while the Ru film showed the lowest immunity to O₃ etching. This may be due to the much faster reaction kinetics for the reaction RuO₂ + O₃ → RuO₄ compared with that of the oxidation speed of Ru by the oxygen radical decomposed from O₃. Therefore, it was identified that the in-situ formation of a thin RuO₂ layer underneath the growing TiO₂, which drove the transformation of the TiO₂ phase from anatase to rutile and is highly desirable for a high dielectric constant, was due to the suppression of direct contact between Ru and O₃ by the intervening TiO₂. The oxygen radical formed on the TiO₂ surface could diffuse onto the Ru surface beneath the TiO₂, and could form RuO₄.

Acknowledgements

The authors appreciate K-MAC MEIS development team for ToF-MEIS analysis and valuable discussion. This study was supported by the Future Semiconductor Device Technology Development Program (10047231) funded by the Ministry of Trade, Industry & Energy of Korea (MOTIE) and the Korea Semiconductor Research Consortium, and Nano-Convergence Foundation funded by the Ministry of Science, ICT and Future Planning (MSIP, Korea) & MOTIE, Korea [Project Name: Development of mass production technology for DRAM capacitor].

Notes and references

^a Department of Materials Science and Engineering and Inter-university Semiconductor Research Center, Seoul National University, Seoul 151-742, Republic of Korea

*E-mail : cheolsh@snu.ac.kr

^b Advanced Materials Division, Korea Research Institute of Chemical Technology, Daejeon 305-600, Republic of Korea

^c Electronic Materials Research Center, Korea Institute of Science and Technology, Seoul 136-791, Republic of Korea

1. S. M. George, *Chem. Rev. (Washington, DC, U. S.)*, 2009, **110**, 111-131.
2. S. M. George, A. W. Ott and J. W. Klaus, *J. Phys. Chem.*, 1996, **100**, 13121-13131.
3. M. Leskelä and M. Ritala, *Thin Solid Films*, 2002, **409**, 138-146.
4. R. L. Puurunen, *J. Appl. Phys.*, 2005, **97**, 121301.
5. T. Suntola, *Thin Solid Films*, 1992, **216**, 84-89.
6. C. S. Hwang, in *Atomic Layer Deposition of Nanostructured Materials*, Wiley-VCH Verlag GmbH & Co. KGaA, 2011, pp. 159-192.
7. C. S. Hwang, *Atomic Layer Deposition for Semiconductors*, Springer US, New York, 2014.
8. M. Ahonen, M. Pessa and T. Suntola, *Thin Solid Films*, 1980, **65**, 301-307.
9. M. Todorova, W. X. Li, M. V. Ganduglia-Pirovano, C. Stampfl, K. Reuter and M. Scheffler, *Phys. Rev. Lett.*, 2002, **89**, 096103.

10. M. Tallarida, K. Kukli, M. Michling, M. Ritala, M. Leskelä and D. Schmeisser, *Chem. Mater.*, 2011, **23**, 3159-3168.
11. S. W. Lee, J. H. Han, S. K. Kim, S. Han, W. Lee and C. S. Hwang, *Chem. Mater.*, 2011, **23**, 976-983.
12. W. Lee, J. H. Han, W. Jeon, Y. W. Yoo, S. W. Lee, S. K. Kim, C.-H. Ko, C. Lansalot-Matras and C. S. Hwang, *Chem. Mater.*, 2013, **25**, 953-961.
13. S.-J. Won, S. Suh, S. W. Lee, G.-J. Choi, C. S. Hwang and H. J. Kim, *Electrochem. Solid-State Lett.*, 2010, **13**, G13-G16.
14. S. K. Kim, W. D. Kim, K. M. Kim, C. S. Hwang and J. Jeong, *Appl. Phys. Lett.*, 2004, **85**, 4112-4114.
15. S. K. Kim, S. Han, G. H. Kim, J. H. Jang, J. H. Han and C. S. Hwang, *J. Electrochem. Soc.*, 2011, **158**, D477-D481.
16. K. Fröhlich, J. Aarik, M. Ľapajna, A. Rosová, A. Aidla, E. Dobročka and K. Hušková, *Journal of Vacuum Science & Technology B*, 2009, **27**, 266-270.
17. S. K. Kim, S. W. Lee, J. H. Han, B. Lee, S. Han and C. S. Hwang, *Adv. Funct. Mater.*, 2010, **20**, 2989-3003.
18. J. H. Han, S. W. Lee, S. K. Kim, S. Han, C. S. Hwang, C. Dussarrat and J. Gatineau, *Chem. Mater.*, 2010, **22**, 5700-5706.
19. J. H. Han, S. W. Lee, G.-J. Choi, S. Y. Lee, C. S. Hwang, C. Dussarrat and J. Gatineau, *Chem. Mater.*, 2008, **21**, 207-209.
20. H. K. Kim, I. H. Yu, J. H. Lee, T. J. Park and C. S. Hwang, *ACS Appl. Mater. Interfaces*, 2013, **5**, 1327-1332.
21. T. Aaltonen, M. Ritala, K. Arstila, J. Keinonen and M. Leskelä, *Chem. Vap. Deposition*, 2004, **10**, 215-219.
22. S. Y. Kang, H. J. Lim, C. S. Hwang and H. J. Kim, *J. Electrochem. Soc.*, 2002, **149**, C317-C323.
23. S. K. Kim, S. Y. Lee, S. W. Lee, G. W. Hwang, C. S. Hwang, J. W. Lee and J. Jeong, *J. Electrochem. Soc.*, 2007, **154**, D95-D101.
24. T. Shibutami, K. Kawano, N. Oshima, S. Yokoyama and H. Funakubo, *Electrochem. Solid-State Lett.*, 2003, **6**, C117-C119.
25. J. H. Han, S. W. Lee, S. K. Kim, S. Han, W. Lee and C. S. Hwang, *Chem. Mater.*, 2012, **24**, 1407-1414.
26. M. Popovici, A. Delabie, C. Adelman, J. Meersschant, A. Franquet, M. Tallarida, J. van den Berg, O. Richard, J. Swerts, K. Tomida, M.-S. Kim, H. Tielens, H. Bender, T. Conard, M. Jurczak, S. Van Elshocht and D. Schmeisser, *ECS J. Solid State Sci. Technol.*, 2013, **2**, N23-N27.
27. B. Hudec, K. Hušková, A. Rosová, J. Šoltýs, R. Rammula, A. Kasikov, T. Uustare, M. Mičušík, M. Omastová, J. Aarik and K. Fröhlich, *J. Phys. D: Appl. Phys.*, 2013, **46**, 385304.
28. A. Böttcher and H. Niehus, *J. Chem. Phys.*, 1999, **110**, 3186-3195.
29. R. Methaapanon, S. M. Geyer, S. Brennan and S. F. Bent, *Chem. Mater.*, 2013, **25**, 3458-3463.
30. R. Methaapanon, S. M. Geyer, H.-B.-R. Lee and S. F. Bent, *J. Mater. Chem.*, 2012, **22**, 25154-25160.
31. B. Chakraborty, S. Holloway and J. K. Nørskov, *Surf. Sci.*, 1985, **152-153, Part 2**, 660-683.
32. M. Nakahara, S. Tsunekawa, K. Watanabe, T. Arai, T. Yunogami and K. Kuroki, *Journal of Vacuum Science & Technology B*, 2001, **19**, 2133-2136.
33. J. Swerts, M. M. Salimullah, M. Popovici, M.-S. Kim, M. A. Pawlak, A. Delabie, M. Schaekers, K. Tomida, B. Kaczer, K. Opsomer, C. Vrancken, I. Debusschere, L. Altimime, J. A. Kittl and S. Van Elshocht, *ECS Trans.*, 2011, **41**, 41-51.
34. J. H. Han, S. Han, W. Lee, S. W. Lee, S. K. Kim, J. Gatineau, C. Dussarrat and C. S. Hwang, *Appl. Phys. Lett.*, 2011, **99**, 022901.
35. S. K. Kim, G. J. Choi, S. Y. Lee, M. Seo, S. W. Lee, J. H. Han, H. S. Ahn, S. Han and C. S. Hwang, *Adv. Mater. (Weinheim, Ger.)*, 2008, **20**, 1429-+.